Ising-type ferroelectric switching and piezoelectric response in wurtzite KMgP: First-principles study

A. Labdelli[a,b,*], and A. Benbedra[b]

[a] *Biodiversity, Water and Soil Conservation Laboratory (LBCES), University of Mostaganem, Algeria,*
[b] *Faculty of Medicine, University of Mostaganem, Algeria*
[*] *e-mail: abbes.labdelli@univ-mosta.dz*

Received 24 june 2026; accepted 27 july 2026

The present paper employs first-principles calculations based on density functional theory to investigate the structural, electronic, ferroelectric, and piezoelectric properties of KMgP in the wurtzite LiGaGe-type phase. The thermodynamical, mechanical and dynamical stability of the compound are confirmed through the formation energy, elastic coefficients and phonon spectrum, respectively. Our results reveal that wurtzite KMgP is a semiconductor with a direct band gap of 1.25 eV within the local-density approximation. We use the Berry-phase approach to evaluate the polarization properties inherent to the polar structure of KMgP, yielding a spontaneous polarization of 0.385 C/m^2 and Born effective charges near their nominal ionic values. The ferroelectric nature of the material is demonstrated by the characteristic double-well potential associated with Ising-type polarization reversal. With a high Curie temperature (385.32 K) and low switching energy barrier (0.0568 eV) and coercive electric field (2.78 MV/cm), we predict that wurtzite KMgP possesses highly reversible polarization, making it a promising candidate for novel ferroelectric applications. Moreover, we find that KMgP is an anomalous piezoelectric compound with a negative longitudinal piezoelectric coefficient (modulus) of -0.75 C/m^2 (-52.66 pC/N).

Keywords: Wurtzite crystals; electric polarization; Berry phase; ferroelectricity; piezoelectricity.

DOI: https://doi.org/10.31349/RevMexFis.72.061008

1. Introduction

Materials that are both piezoelectric and ferroelectric [1] have revolutionized the landscape of solid-state devices. This is due to their unique ability to interconvert electric polarization into mechanical strain on one hand [2,3], and maintain a switchable polarization on the other hand [4,5]. The electromechanical conversion is indispensable for a broad range of applications, including transducers [6], energy harvesters [7], pressure sensors [8] and surface/bulk acoustic wave resonators [9]. Furthermore, the ferroelectric switching is the basis of non-volatile random-access memories, for which 1 and 0 bits correspond to "up" and "down" polarized states [10,11].

Historically, materials crystallizing in the wurtzite structure have been key players in the piezoelectric industry. Binary III-nitrides (such as AlN and GaN) and II-oxides (such as ZnO), along with their various alloys, are widely employed owing to their significant piezoelectric response [12-14]. While these binary compounds are naturally piezoelectric due to their non-centrosymmetric structure, they typically lack the ability for ferroelectric switching under an applied electric field. However, recent studies have demonstrated that some wurtzite crystals can exhibit ferroelectricity [15-19], and thus sparking an interest in identifying new ferroelectric wurtzite compounds.

Promising candidates in that respect are new ternary ABC compounds that crystallize in the wurtzite-like LiGaGe-type phase. Unlike their binary counterparts, these ternary systems offer greater chemical flexibility and a polar ground state that supports both piezoelectricity and ferroelectricity. Bennett *et al*. [20] used first-principles calculations to identify 17 compounds in this structural family, including LiBeP, NaMgAs, NaZnSb and KMgSb. These wurtzite ferroelectrics may be promising for the development of newhigh-performance systems for practical piezoelectric and ferroelectric applications.

In this work, we introduce and investigate the new ternary wurtzite compound KMgP. As far as we know, this material has never been studied before in the literature, particularly regarding its ferroelectric and piezoelectric behaviour. We carry out a density-functional theory (DFT) simulation to predict some physical properties of wurtzite KMgP. We provide results for the structural optimization via total-energy calculations and assess the structural stability through formation energy, elastic constants and phonon frequencies.We further characterize the electronic structure in terms of the band structure and density of states (DOS). A central focus is placed on properties related to electric polarization, namely the spontaneous polarization, Born effective charges and piezoelectric coefficients, all calculated using the Berry-phase theory.We also investigate the Ising-type ferroelectric switching by mapping the double potential well, which allows us to provide critical ferroelectric parameters such as the switching barrier energy, Curie temperature and the coercive electric field. The remainder of the paper is structured as follows. Section 2 details the numerical parameters of the DFT simulation. Section 3 presents our results, subdivided

into three key parts: Sec. 3.1 covers structural optimization, Sec. 3.2 examines structural stability, Sec. 3.3 describes the electronic structure, and Sec. 3.4 explores the ferroelectric switching mechanism and polarization-related quantities. Finally, our findings and concluding remarks are summarized in Sec. 4.

2. Computational details

Ab-initio calculations for wurtzite KMgP are performed within the framework of DFT [21,22] using the WIEN2k package [23], based on the full-potential linearized augmented plane wave plus local orbitals (FP-LAPW+lo) method [24]. In this approach, the unit cell is divided into non-overlapping muffin-tin (MT) spheres and an interstitial region. Inside the MT spheres, the wave functions are expanded in spherical harmonics and radial functions, while plane waves are used in the interstitial region [24]. The exchange-correlation effects are treated using the local-density approximation (LDA) [25]. This choice was adopted to maintain consistency with the seminal first-principles study of LiGaGe-type ferroelectric semiconductors by Bennett *et al*. [20], in which LDA was successfully employed to describe the equilibrium crystal structures, spontaneous polarization, and ferroelectric switching of this class of materials. Since the present work focuses on the ferroelectric and piezoelectric properties of the LiGaGe-type KMgP compound, the use of the same exchange-correlation functional enables a direct and meaningful comparison with the reference study.

Regarding the convergence parameters, the maximum angular momentum inside the MT spheres is set to $l_{\max} = 10$. The plane wave cutoffs are chosen as $RMTK_{\max} = 7$ and $G_{\max} = 12$, where RMT , Kmax and Gmax are defined in Ref. [23]. The core-valence energy separation is fixed at -6 Ry. The valence electron configurations considered are K ($4s^1$), Mg ($3s^2$), and P ($3s^2 3p^3$). The radii RMT of MT spheres of individual elements are chosen as follows: 2.4, 1.9, and 1.85 Bohr for K, Mg, and P, respectively. The Brillouin zone is sampled using 4000 k-points. Total-energy is considered to be converged when the difference is less than 10^{-4} Ry and the forces on atoms are below 10^{-4} Ry/Bohr. The elastic constants are calculated using the energy-strain method as implemented in the IRelast code [26]. Phonon frequencies are obtained using the finite-displacement supercell approach with the Phonopy package [27]. Finally, the polarization properties are evaluated using the BerryPI code [28], interfaced with WIEN2k, within the framework of the modern theory of polarization based on the Berry-phase formalism. The Berry-phase calculations were performed using the converged self-consistent electronic structure obtained with an energy convergence criterion of 10^{-4} Ry. A dense $10 \times 10 \times 40$ Monkhorst-Pack k-point mesh was employed to ensure the numerical convergence of the calculated spontaneous polarization.

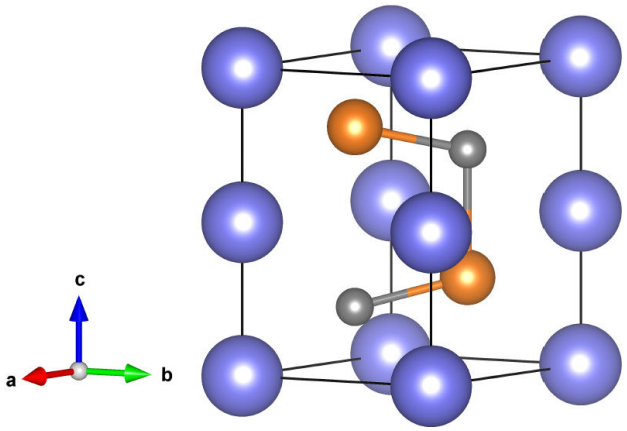


FIGURE 1. Unit cell of KMgP in the non-centrosymmetric polar wurtzite structure. The violet, orange and gray spheres represent K, Mg and P atoms, respectively. The Wyckoff positions are: K at $2a$ (0, 0, 0), Mg at $2b$ (1/3, 2/3, u) and P at $2b'$ (1/3, 2/3, v). The lattice axes a, b, and c are indicated on the left.

3. Results and discussion

3.1. Structural optimization

KMgP is experimentally observed to adopt the tetragonal structure (space group P4/nmmorNo. 129) [29]. Here,we investigate KMgP within the hexagonal wurtzite structure, also known as the LiGaGe-type phase (space groupP63mc, No. 186), whose unit cell is shown in Fig. 1. This structure is described by two independent lattice constants a and c (the lattice angle $\gamma = 120°$). In this case, the equilibrium structural parameters are determined by minimizing the total energy with respect to the unit-cell volume and the lattice constant ratio c/a [30]. The total energy is obtained from self-consistent solutions of the Kohn-Sham equation [31]. The variations of energy as a function of volume and c/a ratio are presented in Fig. 2.

The $E(V)$ data [Fig. 2a)] is fitted using the Murnaghan equation of state [32]:

$$E(V) = E_0 + \frac{BV}{B'}\left[\frac{1}{B'-1}\left(\frac{V}{V_0}\right)^{B'} + 1\right] - \frac{BV_0}{B'-1'}, \quad (1)$$

where E_0 and V_0 denote the equilibrium energy and volume, respectively, B is the bulk modulus, and B' is the first derivative of B with respect to pressure.

On the other hand, the $E(c/a)$ data [Fig. 2b)] is fitted to a fourth-order polynomial of the form:

$$E\left(\frac{a}{c}\right) = k_0 + k_1\left(\frac{a}{c}\right) + k_2\left(\frac{a}{c}\right)^2 + k_3\left(\frac{a}{c}\right)^3 + k_4\left(\frac{a}{c}\right)^4, \quad (2)$$

where k_i are fitting coefficients. The equilibrium lattice constants are obtained from the minimum of the total energy,

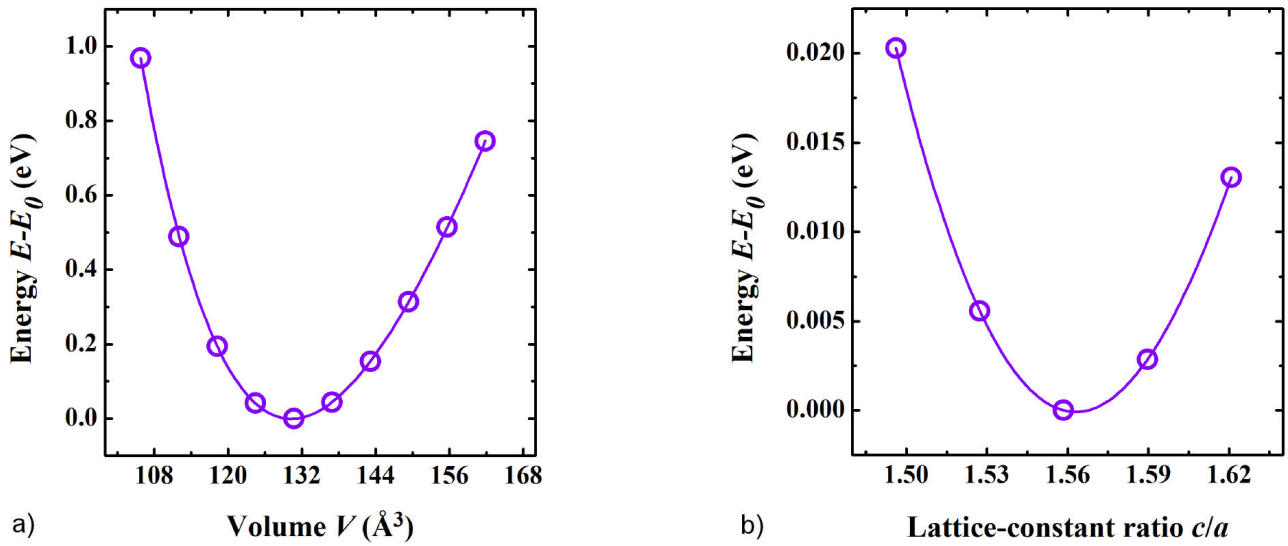


FIGURE 2. Total energy of wurtzite KMgP as a function of a) unit-cell volume and b) lattice-constant ratio c/a. In both cases, the energy scale is referenced to the minimum energy E_0. The curve in a) is a fit to the Murnaghan equation, whereas that in b) corresponds to a fourth-order polynomial fit.

TABLE I. Calculated equilibrium cell volume V, lattice constants a and c, bulk modulus B, its pressure derivative B', and internal parameter u (in units of c) for wurtzite KMgP within the LDA. These values are obtained from total-energy calculations.

KMgP	$V(\text{Å}^3)$	a (Å)	c (Å)	B (GPa)	B'	u	v
	879.9547	4.58	7.16	45.5453	4.309	0.307	0.705

corresponding to the optimal volume V_0 and lattice-constant ratio $(c/a)0$.

For the wurtzite structure, the unit-cell volume is given by

$$V_0 = \frac{\sqrt{3}}{2} a^2 c, \tag{3}$$

from which the lattice constants a and c are determined by:

$$a = \left[\frac{2V_0}{\sqrt{3}(c/a)_0}\right]^{1/3}, \quad c = a(c/a)_0. \tag{4}$$

In addition to the lattice parameters, wurtzite KMgP possesses internal structural degrees of freedom associated with the atomic positions: two internal parameters u and v corresponding to the non-ideal fractional coordinates of the Mg and P atoms along the c-axis [20-33], which cannot be expressed as simple rational fractions.

The equilibrium values of the internal parameters are determined by minimizing the forces acting on the atoms, in accordance with the Hellmann-Feynman theorem [34], *i.e.*, by evaluating the gradients of the total energy with respect to the atomic coordinates. The atomic positions are fully relaxed until the forces converge to negligible values. Note that the K atom occupies the ideal Wyckoff positions (0,0,0) and therefore is not subjected to relaxation.

The calculated equilibrium volume, lattice constants, bulk modulus, its pressure derivative, and the internal parameters for wurtzite KMgP are summarized in Table I. There is no data to compare our values with, since this work is the first to report the structural parameters of wurtzite KMgP. The calculated pressure derivative of the bulk modulus B' is 4.309, which is consistent with the general trend that this parameter remains below 5 for most crystalline solids [35]. The internal parameter $u(v)$ is greater (lesser) than the ideal values 0.25 (0.75).

3.2. Structural stability

Whether or not a material is thermodynamically stable depends on its formation energy (E_f). At $T = 0$ K, it is calculated from total energies as [36]:

$$E_f = E_{\text{KM}_g\text{P}} - \sum_i n_i E_i, \tag{5}$$

where $E_{\text{KM}_g P}$ is the energy of KM$_g$P in the wurtzite structure, $n_i = 2$ is the number of K, Mg and P atoms within KMgP and E_i is the energy per atom of each element in its ground-state bulk structure (tetragonal for K, hexagonal for Mg and orthorhombic for P). We find a formation energy of -1.55 eV per formula unit (f.u.). The negative value indicates that wurtzite KMgP is thermodynamically stable relative to its isolated constituent elements and confirms the possibility of synthesis in the laboratory [36]. We note that KMgP has been experimentally realized only in the tetragonal phase.

Next, we investigate the mechanical stability. This is determined by the elastic constants (C_{ij}). Having hexagonal

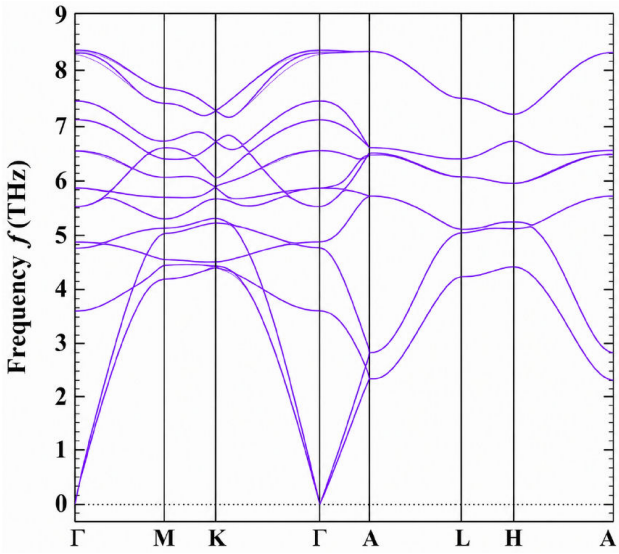


FIGURE 3. Phonon spectrum of KMgP in the wurtzite structure. The horizontal dotted line indicates zero frequency.

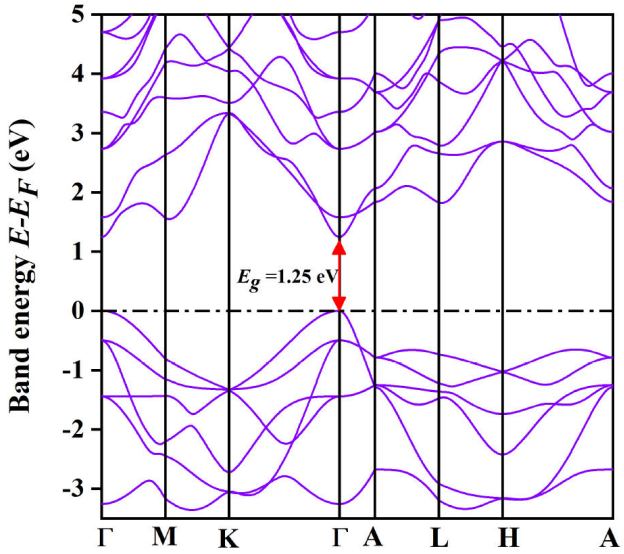


FIGURE 4. Band structure of wurtzite KMgP at the level of LDA. The energy bands are plotted relative to the Fermi level E_F (presented by the dashed horizontal line). The red double arrow indicates the band gap E_g.

symmetry, KMgP has five independent elastic constants. The determination of C_{ij} relies on evaluating the energy under appropriate deformations [37]. We implement such deformations using the IRelast code [26]. The calculated elastic constants of wurtzite KMgP are: $C_{11} = 92.88$ GPa, $C_{12} = 32.33$ GPa, $C_{13} = 31.42$ GPa, $C_{33} = 41.16$ GPa and $C_{44} = 45.31$ GPa.

The elastic constants are doubly interesting. On the one hand, they provide access to several elastic properties that describe the mechanical behaviour of materials, such as the bulk modulus and Poisson ratio. On the other hand, they make it possible to verify the mechanical stability of the system via the Born stability criteria. For a hexagonal crystal, these criteria are [38]:

$$\begin{aligned} C_{11} - C_{12} &> 0, \\ C_{33}(C_{11} + C_{12}) - 2C_{13}^2 &> 0, \\ C_{44} &> 0. \end{aligned} \tag{6}$$

According to our numerical data, the elastic constants satisfy the stability conditions, which implies that the ternary compound KMgP in the wurtzite structure is mechanically stable [38], in the sense that it will not collapse under applied strain.

Finally, we check the dynamical stability. To do so, we calculate the phonon frequencies from the force constants via the Phonopy code [27]. The phonon dispersion curves for wurtziteKMgPare plotted in Fig. 3. The key observation is the absence of any negative (imaginary) frequencies: all phonon modes have positive values of frequency across the entire Brillouin zone, confirming the dynamical stability of KMgP crystallizing in the wurtzite LiGaGe-type phase [39]. In this context, dynamical stability refers to the fact that the crystal structure is stable against its own atomic vibrations.

3.3. Electronic properties

The physical properties of a material are largely governed by its electronic structure. Therefore, understanding the band structure and DOS is essential for identifying materials with potential technological applications.

3.3.1. Band structure

Figure 4 shows the electronic band structure of wurtzite KMgP calculated along the high-symmetry directions of the hexagonal Brillouin zone, with the Fermi level set to zero. As observed in Fig. 4, the valence-band maximum and the conduction-band minimum are both located at the Γ point, revealing a direct band gap. This confirms the semiconducting nature of KMgP. The LDA-predicted band gap is approximately 1.25 eV. The presence of a direct band gap is particularly advantageous for optoelectronic applications, as it enables efficient interband optical transitions. The valence bands, located below the Fermi level, exhibit moderate dispersion, suggesting a mixture of localized and delocalized electronic states. In contrast, the conduction bands are more dispersive, indicating relatively low electron effective masses and potentially high carrier mobility. Furthermore, the variation in band dispersion along different high-symmetry paths $\Gamma - M - K - \Gamma - A - L - H - A$ highlights the anisotropic electronic behaviour associated with the hexagonal wurtzite structure.

3.3.2. Density of states

The total DOS and partial DOS (PDOS) of wurtzite KMgP are shown in Figs. 5 and 6, respectively. The absence of elec-

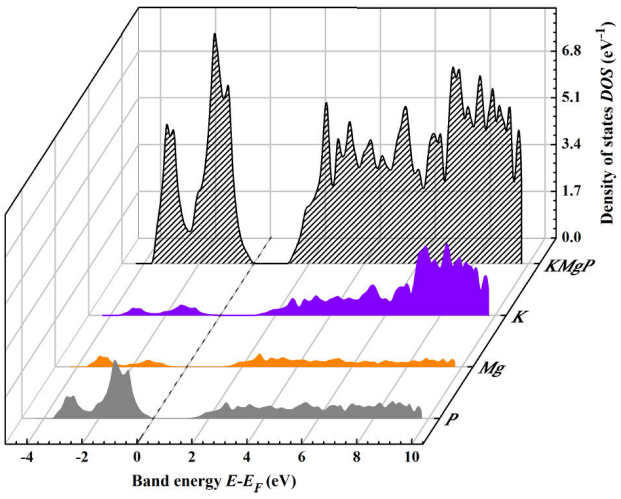


FIGURE 5. Total and atomic-projected DOS for KMgP in the wurtzite structure (within LDA). The dashed area represents the total DOS of the system. The violet, orange, and grey areas are the K , Mg, and P contributions, respectively. As in Fig. 4, the energy is referenced to the Fermi level dashed black line that passes the zero energy.

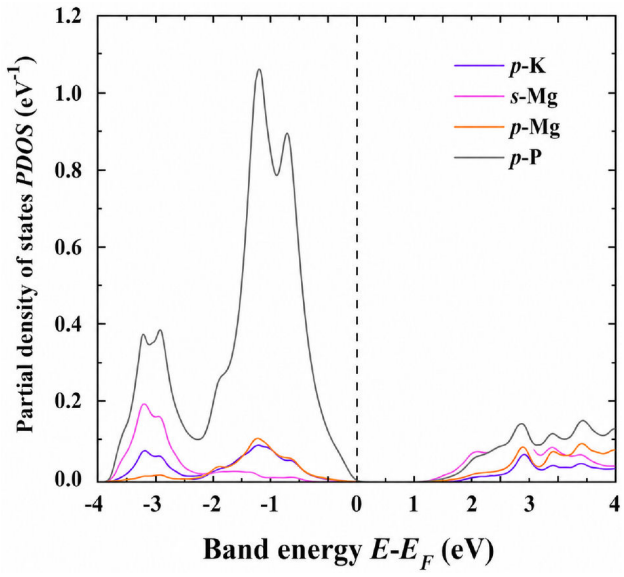


FIGURE 6. Orbital-projected PDOS of wurtzite KMgP. The vertical dashed line indicates the Fermi level.

tronic states at the Fermi level confirms the semiconducting nature of our compound, in agreement with the band-structure results. By inspecting Fig. 6, we observe that the valence band region (from approximately -4 eV to 0 eV) is mainly dominated by P-p states, which provides the major contribution near the valence-band maximum. Smaller contributions from K-s and Mg-s states are also observed, indicating a certain degree of hybridization between P and the metallic atoms. This hybridization suggests a mixed bonding character with partial covalent features. In the conduction band region (above the Fermi level), the electronic states are primarily composed of Mg-s, Mg-p, and P-p states, with minor contributions from K-p states. This indicates that the conduction-band minimum is mainly derived from the metal atoms, consistent with the relatively dispersive conduction bands observed in the band structure. Moreover, the sharp peaks in the DOS correspond to localized states, while the broader features indicate more delocalized electronic states.

3.4. Electric polarization

3.4.1. Spontaneous polarization

The spontaneous polarization (PSP) of a crystalline solid is the value of polarization at equilibrium, *i.e.* in the absence of external perturbations such as electric field and mechanical strain. The theoretical framework to define and compute the electric polarization is the Berry-phase theory [40,41], which is based on two fundamental hypotheses [42,43]: (i) the only physically meaningful values of polarization are polarization differences between two different states, and (ii) such polarization differences are calculated as a Berry phase of the system wavefunction. For the spontaneous polarization, the two states correspond to a non-centrosymmetric structure and its high-symmetry counterpart, also referred to as the reference structure [42,43].

In the specific case of our compound KMgP, the non-centrosymmetric structure is wurtzite whereas the structure that serves as a reference is the layered-hexagonal phase [20-44]. The latter structure can be constructed from the wurtzite phase by putting the cations and anions on the same atomic plane (*i.e.* $u = 0.25$ and $v = 0.75$) [20]. Hence the spontaneous polarization is calculated as the difference between the polarization of the wurtzite (LiGaGe-type) and layered-hexagonal (ZrBeSi-type) structures:

$$P_{\mathrm{SP}} = P_{\mathrm{WZ}} - P_{\mathrm{LH}}, \tag{7}$$

where P_{WZ} and P_{LH} refer to the wurtzite and layered-hexagonal polarization values, respectively, both of which are evaluated as a Berry phase of the Bloch-like orbitals via the BerryPI code.

The value of the spontaneous polarization of wurtzite KMgP is found to be 0.385 C/m^2. Note that polarization is a vector quantity. Due to hexagonal symmetry, the polarization vector is always along the vertical c-axis. The positive value of P_{SP} indicates that the spontaneous polarization vector points to the [0001] direction.

The spontaneous polarization of KMgP is benchmarked to previously reported LiGaGe-type ferroelectrics. We choose the two related materials KMgSb and NaMgP as comparative case-studies. This allows us to investigate the effect of chemical substitution on polarization properties. The spontaneous polarization is (0.370 C/m^2) for KMgSb [45] and (0.490 C/m^2) for NaMgP [20]. Both values are within the same order of magnitude as the value calculated for KMgP (0.385 C/m^2).

TABLE II. Born effective charges Z^* (in unit of e) of individual ions (K, Mg and P) for wurtzite KMgP with their nominal values Z.

	K	Mg	P
Z^*	0.71	2.1	-2.80
Z	1	2	-3

3.4.2. *Born effective charge*

The Born effective charge (Z^*) describes the polarization induced by ionic displacements [45]. Within the Berry-phase method, the calculation of the Born effective charge is done by studying the variation of polarization as the different ions are displaced from their equilibrium positions [46,47]:

$$Z_i^* = \frac{V}{e}\frac{\Delta P_i}{\Delta r_i}, \tag{8}$$

where V is the unit cell volume, e is the electron charge, ΔP_i is the change in polarization that results from the ionic displacement Δr_i and i runs over each ion (K, Mg and P). In our study, we introduce for each ion a small displacement of ± 0.1 % along the c-axis and calculate the corresponding polarizations as Berry phases. The results for the Born effective charges of wurtzite KMgP are gathered in Table II. The nominal ionic charges Z are also included for the sake of comparison.

It can be seen that the effective charge of each ion has the same sign as and is very close to the nominal value (especially for Mg and P). It is established that the approximate equivalence of Z^* and Z is an indicator of a strong ionic character of the chemical bonds [47,48], which aligns with the large value of the spontaneous polarization reported above. In order to verify the validity of our simulation we check the acoustic sum rule, which states that the sum of the effective charge of all ions in the unit cell is zero [49]. Our values of Z^* obey this rule to a negligible error (see Table II).

3.4.3. *Ferroelectric switching*

Acondensed system is ferroelectric if its polarization vector can be reversed by an external electric field [50]. In what follows, we demonstrate that KMgP is one of the wurtzite materials that support ferroelectricity. For this purpose, we present in Fig. 7 the variation of energy as a function of the reaction coordinate.We observe a double potentialwell that characterizes the Ising-type polarization reversal by 180°. There exist other ferroelectric switching mechanisms such as the Bloch- and Néel-types, in which the polarization vector does not vanish but rather rotates by an angle [51]. The reaction coordinate x describes the shift of the cation Mg and anion P up and down the c-axis, with $x = 1$ and $x = -1$ corresponding to the ferroelectric wurtzite structures with opposite polarization (the two minima in Fig. 7) [52]. To study ferroelectric switching a paraelectric state of well-defined polarization is needed. For wurtzite ferroelectrics, a straightforward choice would be the layered-hexagonal configuration, for which $x = 0$ [52] (the saddle point in Fig. 7).

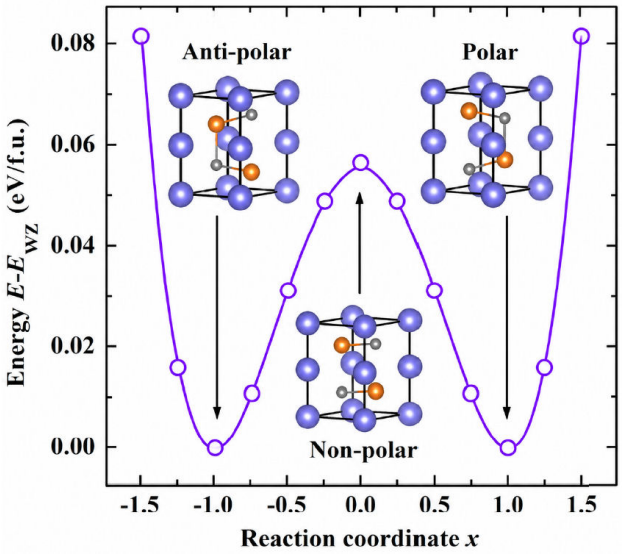


FIGURE 7. Energy per formula unit of wurtzite KMgP as a function of the reaction coordinate x, which controls ionic displacements along the c-axis. The origin of energy is taken to be the energy of the ferroelectric configuration E_{WZ}. The inset shows hexagonal unit cells corresponding to the polar wurtzite (1), layered-hexagonal (2), and anti-polar wurtzite (3) structures.

The energy profile allows us to extract important parameters associated with the ferroelectric effect. The height of the potentialwell is the energy barrier (US) against polarization switching, which is equal to the energy difference between the ferroelectric and paraelectric states [53]:

$$U_S = E_{\text{LH}} - E_{\text{WZ}}, \tag{9}$$

where LH and WZ denote the layered-hexagonal (paraelectric) and wurtzite (ferroelectric) values, respectively. Our prediction of U_S for KMgP is 0.0568 eV/f.u. This energy barrier is small enough that an applied electric field can reverse the polarization vector. For the sake of comparison, the switching barrier of wurtzite KMgSb and NaMgP is reported to be 0.093 [45] and 0.20 eV/f.u. [20], respectively. Another ferroelectric parameter is the Curie temperature (TC), defined as the temperature beyond which the material loses its ferroelectric behaviour [54]. For typical ferroelectric compounds, the value of TC can be approximated by:

$$T_C = \frac{U_S}{k_B}, \tag{10}$$

with k_B being the Boltzmann constant. Using this formula, the Curie temperature of wurtziteKMgPis 385.32 K, which is higher than room temperature (300 K). This is essential for practical applications, since KMgP-based ferroelectric devices usually operate under normal conditions of pressure and temperature. The Curie temperature for KMgSb and NaMgP were not reported in Refs. [20,45]. However, we can use the switching barriers and Eq. (9) to predict its value for both

systems: 1078.26 K for KMgSb and 2318.84 KforNaMgP. The value of T_C can be seen to be much larger for KMgSb and NaMgP than for KMgP. This is consistent with the trend identified earlier, since the switching barrier increases in going from KMgP to KMgSb and NaMgP, and it is obvious from Eq. (9) that this effect tends to increase the Curie temperature.

It is important to emphasize that Eq. (9) provides only a rough qualitative estimate of the Curie temperature. Because it relies on a local mean-field approximation, it does not account for spatial thermal fluctuations and long-range dipole-dipole interactions. For a quantitative and physically rigorous determination of T_C, more sophisticated statistical mechanics approaches, such as constructing an effective Hamiltonian or performing large-scale Monte Carlo simulation [56], are required. Nevertheless, this simple relation gives a first approximation for the value of T_C for KMgP and similar wurtzite ferroelectrics.

Finally, we define the coercive electric field (E_C) to be the minimum field required to switch the polarization. Using the values of P_{SP} and U_S, the intensity of E_C is estimated via [57]:

$$E_C = \frac{8}{3\sqrt{3}} \frac{U_S}{V P_{\text{SP}}}. \tag{11}$$

We point out that this value represents the ideal intrinsic coercive field derived from assuming a homogeneous switching mechanism across a defect-free crystal. In real experimental measurements, polarization reversal typically occurs at significantly lower electric fields [57] . This discrepancy is well known in ferroelectrics and stems from the fact that experimental switching is a heterogeneous process mediated by the nucleation and motion of domains at defects, impurities and grain boundaries. This leads to a reduced energy barrier and, consequently, reduced coercivity compared to the homogenous process.

We find that a coercive field of about 2.78 MV/cm is needed to reverse the polarization from "up" to "down" and vice versa. Because this coercive field is moderate, polarization in wurtzite KMgP is expected to switch before reaching the dielectric breakdown limit (the threshold where the material fails as an insulator and its polarization vanishes).

Based on the values of PSP and US given in Refs. [20,45], the intrinsic coercive field for KMgSb and NaMgP is computed to be 3.56 and 8.63MV/cm, respectively. Both values are smaller than that of KMgP. This ordering is consistent with the values of the switching barrier and spontaneous polarization for the three materials [see Eq. (10)].

3.4.4. Piezoelectric coefficients

Piezoelectricity is the property of some materials to exhibit an electric polarization (called piezoelectric polarization) upon the application of a mechanical deformation [56]. Wurtzite crystals such as KMgP display this effect since their symmetry does not allow a centre of inversion [57]. The piezoelectric response of wurtzite materials is quantified by three independent piezoelectric constants, namely e_{33}, e_{31} and e_{15} [57]. The coefficients e_{33} and e_{31} measure the polarization induced by uniaxial and biaxial strain, respectively. The coefficient e_{15}, on the other hand, links the polarization to shear strain. Given the complexity to implement shear deformation,we carry out calculation of e_{33} and e_{31}. In order to do so,we investigate the evolution of polarization as small strains are applied. A finite difference then leads to values of e_{ij} as follows [58]:

$$e_{3j} = \frac{\Delta P_3}{\Delta \epsilon_j}, \tag{12}$$

where $\Delta\epsilon_j = 1$ % is the applied strain and ΔP_3 is the polarization difference (along the c-axis) between the 0.5% and -0.5 % strained wurtzite structures. The strain index j denotes Cartesian axes within the Voigt notation ($x = 1$ for e_{31} and $z = 3$ for e_{33}). The piezoelectric coefficients of wurtzite KMgP are calculated to be $e_{33} = -0.75$ C/m^2 and $e_{31} = 1.19$ C/m^2. We see that e_{33} (e_{31}) is negative (positive), in sharp contrast with typical wurtzite binaries like AlN, GaN and ZnO, where the signs are reversed between the two coefficients. e_{33} is also negative for KMgSb (-0.42 C/m^2 [61]) but is positive for NaMgP (0.58 C/m^2 [61]).

For the longitudinal piezoelectric constant e_{33}, the negative sign implies that stretching the crystal along the c-axis reduces the polarization, or equivalently, the polarization opposes the applied tensile strain. This unusual piezoelectric behaviour stems from the combination of low Born effective charges (see Table II) and small strain sensitivity of the internal parameters $\partial u/\partial\epsilon\epsilon_3$ and $\partial v/\partial\epsilon_3$ [59]. Indeed, the response of the internal coordinates of KMgP to the applied strain is extremely low, namely $\partial u/\partial\epsilon\epsilon_3 = -0.045$ and $\partial v/\partial\epsilon\epsilon_3 = 0.018$.

The experimental evaluation of the piezoelectric response usually relies on the piezoelectric moduli d_{ij}, rather than the piezoelectric coefficients e_{ij}. The relation between d_{ij} and e_{ij} can readily be found from the elastic coefficients C_{ij} [60]:

$$d_{33} = \frac{e_{33}(C_{11}+C_{12}) - 2e_{31}C_{13}}{(C_{11}+C_{12})C_{33} - 2C_{13}^2},$$
$$d_{31} = \frac{e_{31}C_{33} - e_{33}C_{13}}{(C_{11}+C_{12})C_{33} - 2C_{13}^2}. \tag{13}$$

We obtain the values $d_{33} = -52.66$ pC/N and $d_{31} = 22.72$ pC/N. Due to the absence of prior literature on the piezoelectric coefficients and moduli of this system, a comparative analysis of our results is not possible. We can only compare the present results with previously studied similar compounds. The value of d_{33} is -19.15 pC/N for KMgSb and 7.80 pC/N for NaMgP [61] (there is no data on d_{31}).

4. Conclusion

In this paper, we have conducted a comprehensive first-principles investigation of the structural, electronic, ferroelectric and piezoelectric properties of KMgP within the

wurtzite LiGaGe-type structure. Our results suggest thatK-MgPis a theoretically viable candidate as a functional material in both ferroelectric and piezoelectric applications. The mechanical and dynamical stability of the wurtzite phase was verified, as the calculated elastic constants satisfy the Born criteria and the phonon spectrum exhibit no imaginary frequencies. Electronic-structure calculations identify wurtzite KMgP as a direct-gap semiconductor. DOS analysis revealed that the valence band is primarily composed of P orbitals, while the conduction band is dominated by a mixture of P and Mg states.

Regarding the ferroelectric behaviour of our compound, we employed the Berry-phase technique to determine the spontaneous polarization and the Born effective charges for each constituent ion. Next, we modelled the ferroelectric switching via the double-well potential energy profile. The calculated energy barrier and coercive field indicate that polarization reversal is energetically feasible, confirming the potential forKMgPto be utilized in practical ferroelectric devices.

Finally, we reported the piezoelectric coefficients and moduli, and discussed the counterintuitive negative longitudinal piezoelectric constants e_{33} and d_{33}. Future work will focus on a more comprehensive investigation of the dielectric response, electron localization function (ELF), and hybrid-functional calculations to provide further insight into the electronic structure, chemical bonding, and ferroelectric properties of KMgP.

Competing interests

The authors declare no competing interests.

Data availability statement

The data that support the findings of this study are available from the corresponding author upon reasonable request.

1. R. Machado, M. G. Stachiotti, R. L. Migoni and A. H. Tera, Estructura electrónica y origen de la ferroelectricidad en el Bi4Ti3O12, por medio de cálculos de primeros principios, *Rev. Mex. Fis.* **51** (2005), https://rmf.smf.mx/ojs/index.php/rmf/article/view/3357.
2. M. De Jong, W. Chen, H. Geerlings, M. Asta and K. A. Persson, A database to enable discovery and design of piezoelectric materials, *Sci. Data* **2** (2015), https://doi.org/10.1038/sdata.2015.53.
3. X. Guo, Z. Li, J. Peng, H. Dong, R. Wang, Y. Yang and F. Wu, Piezoelectric properties of novel group III-VI TiA2X4 (A = Ga, Al; X = S, Se, Te) monolayers: First-principles calculations, *Phys. Lett. A* **572** (2026) 131365, https://doi.org/10.1016/j.physleta.2026.131365.
4. H. Fu and R. E. Cohen, Polarization rotation mechanism for ultrahigh electromechanical response in single-crystal piezoelectrics, *Nature* **403** (2000) 281, https://doi.org/10.1038/35002022.
5. X. Ding, J. B. Si, Y. Zhang, L. Tang, J. H. Ma, Y. H. Xie and X. Q. Deng, Electronic properties and device design of ferroelectric Al2O3/GaN heterostructure, *Phys. Lett. A* **497** (2024) 129328, https://doi.org/10.1016/j.physleta.2024.129328.
6. D. A. Aldahiry, D. A. Bajaba, N. M. Basalamah and M. M. Ahmed, Piezoelectric Transducer as an Energy Harvester: A Review, Yemeni *J. Eng. Sci.* **19** (2022) 30, https://doi.org/10.53370/001c.33771.
7. H. Liu, J. Zhong, C. Lee, S.-W. Lee and L. Lin, A comprehensive review on piezoelectric energy harvesting technology: Materials, mechanisms, and applications, *Appl. Phys. Rev.* **5** (2018) 041306, https://doi.org/10.1063/1.5074184.
8. J. Li, L. Fang, B. Sun, X. Li and S. H. Kang, Review-Recent Progress in Flexible and Stretchable Piezoresistive Sensors and Their Applications, *J. Electrochem. Soc.* **167** (2020) 037561, https://doi.org/10.1149/1945-7111/ab6828.
9. L. Wang, C. Wang, Y. Wang, A. Quan, M. Keshavarz, B. P. Madeira, H. Zhang, C. Wang and M. Kraft, A Review on Coupled Bulk Acoustic Wave MEMS Resonators, *Sensors* **22** (2022), https://doi.org/10.3390/s22103857.
10. Y. Arimoto and H. Ishiwara, Current Status of Ferroelectric Random-Access Memory, *MRS Bull.* **29** (2004) 823, https://doi.org/10.1557/mrs2004.235.
11. Y. Kato, T. Yamada and Y. Shimada, 0.18-Î¼m nondestructive readout FeRAM using charge compensation technique, IEEE Trans. *Electron Devices* **52** (2005) 2616, https://doi.org/10.1109/TED.2005.859688.
12. K. R. Talley, R. Sherbondy, A. Zakutayev and G. L. Brennecka, Review of high-throughput approaches to search for piezoelectric nitrides, *J. Vac. Sci. Technol. A* **37** (2019) 060803, https://doi.org/10.1116/1.5125648.
13. N. Gogneau, N. Jamond, P. Chrétien, F. Houzé, E. Lefeuvre and M. Tchernycheva, From single III-nitride nanowires to piezoelectric generators: New route for powering nomad electronics, *Semicond. Sci. Technol.* **31** (2016) 103002, https://doi.org/10.1088/0268-1242/31/10/103002.
14. R. K. Pandey, J. Dutta, S. Brahma, B. Rao and C.-P. Liu, Review on ZnO-based piezotronics and piezoelectric nanogenerators: aspects of piezopotential and screening effect, *J. Phys. Mater.* **4** (2021) 044011, https://doi.org/10.1088/2515-7639/ac130a.
15. Y. Shimomura, S. Ohno, K. Hayashi and H. Akamatsu, Quadruple-well ferroelectricity and moderate switching barrier in defective wurtzite α-Al2S3: a first-principles study, *npj Comput. Mater.* **11** (2025) 38, https://doi.org/10.1038/s41524-025-01519-3.
16. C.-W. Lee, K. Yazawa, A. Zakutayev, G. L. Brennecka and P. Gorai, Switching it up: New mechanisms revealed in wurtzite-type ferroelectrics, *Sci. Adv.* **10** (2024) eadl0848, https://doi.org/10.1126/sciadv.adl0848.

17. S. Fichtner, N. Wolff, F. Lofink, L. Kienle and B. Wagner, AlScN: A III-V semiconductor based ferroelectric, *J. Appl. Phys.* **125** (2019) 114103, https://doi.org/10.1063/1.5084945.
18. D.Wang *et al.*, FerroelectricYAlN grown by molecular beam epitaxy, *Appl. Phys. Lett.* **123** (2023) 033504, https://doi.org/10.1063/5.0159562.
19. A. Konishi, T. Ogawa, C. A. J. Fisher, A. Kuwabara, T. Shimizu, S. Yasui, M. Itoh and H. Moriwake, Mechanism of polarization switching in wurtzite-structured zinc oxide thin films, *Appl. Phys. Lett.* **109** (2016) 102903, https://doi.org/10.1063/1.4962440.
20. J. W. Bennett, K. F. Garrity, K. M. Rabe and D. Vanderbilt, Hexagonal ABC Semiconductors as Ferroelectrics, *Phys. Rev. Lett*. **109** (2012) 167602, https://doi.org/10.1103/PhysRevLett.109.167602.
21. P. Hohenberg and W. Kohn, Inhomogeneous Electron Gas, *Phys. Rev.* **136** (1964) B864, https://doi.org/10.1103/PhysRev.136.B864.
22. R. O. Jones, Density functional theory: Its origins, rise to prominence, and future, *Rev. Mod. Phys.* **87** (2015) 897, https://doi.org/10.1103/RevModPhys.87.897.
23. P. Blaha, K. Schwarz, F. Tran, R. Laskowski, G. K. H. Madsen and L. D. Marks, WIEN2k: An APW+lo program for calculating the properties of solids, *J. Chem. Phys.* **152** (2020) 074101, https://doi.org/10.1063/1.5143061.
24. E. Sjöstedt, L. Nordström and D. J. Singh, An alternative way of linearizing the augmented plane-wave method, *Solid State Commun*. **114** (2000) 15, https://doi.org/10.1016/S0038-1098(99)00577-3.
25. J. P. Perdew and A. Zunger, Self-interaction correction to density-functional approximations for many-electron systems, *Phys. Rev. B* **23** (1981) 5048, https://doi.org/10.1103/PhysRevB.23.5048
26. M. Jamal, M. Bilal, I. Ahmad and S. Jalali-Asadabadi, IRelast package, *J. Alloys Compd.* **735** (2018) 569, https://doi.org/10.1016/j.jallcom.2017.10.139.
27. A. Togo, First-principles Phonon Calculations with Phonopy and Phono3py, *J. Phys. Soc. Jpn*. **92** (2023) 012001, https://doi.org/10.7566/JPSJ.92.012001.
28. S. J. Ahmed, J. Kivinen, B. Zaporzan, L. Curiel, S. Pichardo and O. Rubel, BerryPI: A software for studying polarization of crystalline solids with WIEN2k density functional all-electron package, *Comput. Phys. Commun.* **184** (2013) 647, https://doi.org/10.1016/j.cpc.2012.10.028.
29. R. Vogel and H.-U. Schuster, Neue elektrovalente ternäre Verbindungen des Kaliums mit Magnesium und Elementen der 5. Hauptgruppe, *Z. Naturforsch.* B **34** (1979) 1719, https://doi.org/10.1515/znb-1979-1219.
30. Y.-N. Xu and W. Y. Ching, Electronic, optical, and structural properties of some wurtzite crystals, *Phys. Rev. B* **48** (1993) 4335, https://doi.org/10.1103/PhysRevB.48.4335.
31. W. Kohn and L. J. Sham, Self-Consistent Equations Including Exchange and Correlation Effects, *Phys. Rev.* **140** (1965) A1133, https://doi.org/10.1103/PhysRev.140.A1133.
32. F. D. Murnaghan, The Compressibility of Media under Extreme Pressures, *Proc. Natl. Acad. Sci. U.S.A.* **30** (1944) 244, https://doi.org/10.1073/pnas.30.9.244.
33. F. Casper, C. Felser, R. Seshadri, C. P. Sebastian and R. Pöttgen, Searching for hexagonal analogues of the half-metallic half-Heusler XYZ compounds, *J. Phys. D: Appl. Phys.* **41** (2008) 035002, https://doi.org/10.1088/0022-3727/41/3/035002.
34. R. P. Feynman, Forces in Molecules, *Phys. Rev.* **56** (1939) 340, https://doi.org/10.1103/PhysRev.56.340.
35. A. M. Hofmeister, Pressure derivatives of the bulk modulus, *J. Geophys. Res. Solid Earth* **96** (1991) 21893, https://doi.org/10.1029/91JB02157.
36. V. Stevanović, S. Lany, X. Zhang and A. Zunger, Correcting density functional theory for accurate predictions of compound enthalpies of formation: Fitted elemental-phase reference energies, *Phys. Rev. B* **85** (2012) 115104, https://doi.org/10.1103/PhysRevB.85.115104.
37. D. Holec, M. Friák, J.Neugebauer and P. H.Mayrhofer, Trends in the elastic response of binary early transition metal nitrides, *Phys. Rev. B* **85** (2012) 064101, https://doi.org/10.1103/PhysRevB.85.064101.
38. F. Mouhat and F.-X. Coudert, Necessary and sufficient elastic stability conditions in various crystal systems, *Phys. Rev. B* **90** (2014) 224104, https://doi.org/10.1103/PhysRevB.90.224104.
39. G. Petretto *et al*., High-throughput density-functional perturbation theory phonons for inorganic materials, *Sci. Data* **5** (2018) 180065, https://doi.org/10.1038/sdata.2018.65.
40. R. D. King-Smith and D. Vanderbilt, Theory of polarization of crystalline solids, *Phys. Rev. B* **47** (1993) 1651, https://doi.org/10.1103/PhysRevB.47.1651.
41. R. Resta, Theory of the electric polarization in crystals, *Ferroelectrics* **136** (1992) 51, https://doi.org/10.1080/00150199208016065.
42. R. Resta, Macroscopic Electric Polarization as a Geometric Quantum Phase, *Europhys. Lett.* **22** (1993) 133, https://doi.org/10.1209/0295-5075/22/2/010.
43. R. Resta and D. Vanderbilt, Theory of Polarization: A Modern Approach, in Physics of Ferroelectrics: A Modern Perspective (Springer, Berlin, 2007), pp. 31-68, https://doi.org/10.1007/978-3-540-34591-6_2.
44. C. E. Dreyer, A. Janotti, C. G. Van de Walle and D. Vanderbilt, Correct Implementation of Polarization Constants in Wurtzite Materials and Impact on III-Nitrides, *Phys. Rev. X* **6** (2016) 021038, https://doi.org/10.1103/PhysRevX.6.021038.
45. E. H. Abbes, A. Benbedra, I. Bouhamou, L. Latreche, H. Abbassa and S. Meskine, Stability, Electronic Structure and Ferroelectric Switching of Wurtzite KMgSb, *Phys. Status Solidi B* **263** (2026) e202500633, https://doi.org/10.1002/pssb.202500633.
46. A. Dal Corso *et al*., Ab initio study of piezoelectricity and spontaneous polarization in ZnO, *Phys. Rev. B* **50** (1994) 10715, https://doi.org/10.1103/PhysRevB.50.10715.

47. F. Bernardini, V. Fiorentini and D. Vanderbilt, Spontaneous polarization and piezoelectric constants of III-V nitrides, *Phys. Rev. B* **56** (1997) R10024, https://doi.org/10.1103/PhysRevB.56.R10024.

48. S. Massidda *et al*., Polarization and dynamical charge of ZnO within different one-particle schemes, *Phys. Rev. B* **52** (1995) R16977, https://doi.org/10.1103/PhysRevB.52.R16977.

49. X. Gonze and C. Lee, Dynamical matrices, Born effective charges, dielectric permittivity tensors, and interatomic force constants from density-functional perturbation theory, *Phys. Rev. B* **55** (1997) 10355, https://doi.org/10.1103/PhysRevB.55.10355.

50. K. F. Garrity, High-throughput first-principles search for new ferroelectrics, *Phys. Rev. B* **97** (2018) 024115, https://doi.org/10.1103/PhysRevB.97.024115.

51. D. Lee, R. K. Behera, P. Wu, H. Xu, Y. L. Li, S. B. Sinnott, S. R. Phillpot, L. Q. Chen and V. Gopalan, Mixed Bloch-Néel-Ising character of 180° ferroelectric domain walls, *Phys. Rev. B* **80** (2009) 060102, https://doi.org/10.1103/PhysRevB.80.060102.

52. S. J. Ahmed, S. Pichardo, L. Curiel and O. Rubel, First-principle modelling of the ferroelectric switching in BaTiO3: concurrent switching versus domain wall motion, *Model. Simul. Mater. Sci. Eng*. **22** (2014) 055014, https://doi.org/10.1088/0965-0393/22/5/055014.

53. J. Cole, S. J. Ahmed, L. Curiel, S. Pichardo and O. Rubel, Marble game with optimal ferroelectric switching, *J. Phys.: Condens. Matter* **26** (2014) 135901, https://doi.org/10.1088/0953-8984/26/13/135901.

54. K. M. Rabe, M. Dawber, C. Lichtensteiger, C. H. Ahn and J.-M. Triscone, Modern Physics of Ferroelectrics: Essential Background, in Physics of Ferroelectrics: A Modern Perspective (Springer, Berlin, 2007), pp. 1-30, https://doi.org/10.1007/978-3-540-34591-6_1.

55. S. P. Beckman, X.Wang, K. M. Rabe and D.Vanderbilt, Ideal barriers to polarization reversal and domain-wall motion in strained ferroelectric thin films, *Phys. Rev. B* **79** (2009) 144124, https://doi.org/10.1103/PhysRevB.79.144124.

56. M. C. Sekhar, E. Veena, N. S. Kumar, K. C. B. Naidu, A. Mallikarjuna and D. B. Basha, A Review on Piezoelectric Materials and Their Applications, *Cryst. Res. Technol.* **58** (2023) 2200130,https://doi.org/10.1002/crat.202200130.

57. P. J. Dobson, Physical Properties of Crystals - Their Representation by Tensors and Matrices, *Phys. Bull.* **36** (1985) 506, https://doi.org/10.1088/0031-9112/36/12/027.

58. P. Gopal, N. A. Spaldin and U. V. Waghmare, First-principles study of wurtzite-structure MnO, *Phys. Rev. B* **70** (2004) 205104, https://doi.org/10.1103/PhysRevB.70.205104.

59. S. Liu and R. E. Cohen, Origin of Negative Longitudinal Piezoelectric Effect, *Phys. Rev. Lett.* **119** (2017) 207601, https://doi.org/10.1103/PhysRevLett.119.207601.

60. M. Catti, Y. Noel and R. Dovesi, Full piezoelectric tensors of wurtzite and zinc blende ZnO and ZnS by first-principles calculations, *J. Phys. Chem. Solids* **64** (2003) 2183, https://doi.org/10.1016/S0022-3697(03)00219-1.